FULL PAPER

To be cited as: *Chem. Asian J.* 10.1002/asia.202000679

Link to VoR: https://doi.org/10.1002/asia.202000679

Octanuclear Ni_4Ln_4 Coordination Aggregates from Schiff Base Anion Supports and Connecting of Two Ni_2Ln_2 Cubes: Syntheses, Structures, and Magnetic Properties

Mousumi Biswas,[a] E. Carolina Sañudo[b,c] and Debashis Ray*[a]

[a] M. Biswas, Prof. D. Ray
Department of Chemistry
Indian Institute of Technology
Kharagpur 721 302 (India)
E-mail: dray@chem.iitkgp.ac.in
[b] Prof. E. C. Sañudo
Departament de Química Inorgànica i Orgànica, Universitat de Barcelona, Diagonal 645, 08028 Barcelona SPAIN
[c] Institut de Nanociència i Nanotecnologia, Universitat de Barcelona, (IN2UB) 08028 Barcelona SPAIN

Supporting information for this article is given via a link at the end of the document.

Abstract: A family of 3d-4f aggregates have been reported through guiding the dual coordination modes of ligand anion (HL^-) and *in situ* generated ancillary bridge driven self-assembly coordination responses toward two different types of metal ions. Reactions of lanthanide(III) nitrate (Ln = Gd, Tb, Dy, Ho and Yb), nickel(II) acetate and phenol-based ditopic ligand anion of 2-[{(2-hydroxypropyl)imino}methyl]-6-methoxyphenol (H_2L) in MeCN-MeOH (3:1) mixture and LiOH provided five new octanuclear *Ni-4f* coordination aggregates from two Ni_2Ln_2 cubanes. Single-crystal X-ray diffraction analysis reveals that all the members of the family are isostructural, with the central core formed from the coupling of two distorted $[Ni_2Ln_2O_4]$ heterometallic cubanes $[Ni_2Ln_2(HL)_2(\mu_3\text{-}OH)_2(OH)(OAc)_4]^+$ (Ln = Gd (**1**), Tb (**2**), Dy (**3**), Ho (**4**) and Yb (**5**)). Higher coordination demand of *4f* ions induced the coupling of the two cubes by $(OH)(OAc)_2$ bridges. Variable temperature magnetic study reveals weak coupling between the Ni^{2+} and Ln^{3+} ions. For the Tb (**2**) and Dy (**3**) analogs, the compounds are SMMs, whereas the Gd (**1**) analogue is not an SMM. The observation revealed thus that the anisotropy of the Ln^{3+} ions is central to display the SMM behavior within this structurally intriguing family of compounds.

Introduction

Ligand anion bound multinuclear coordination aggregates of two similar or different types of metal ions form an exclusive class of assemblies, many of which can have visually pleasing molecular designs. Their exciting physical and chemical properties arise primarily from the electronic and/or magnetic interplay between the constituent metal ions of varying numbers trapped by the ligand anions. In recent years the field of molecular magnetism have seen an enormous progress in laboratory-level synthesis following the observation of nanosized Mn_{12} aggregate exhibiting a bistable magnetic ground state and magnetic hysteresis.[1] The gram-scale synthesis of the compound basically laid the foundation for research in improving and perfecting control over the magnetic relaxation of single molecule magnets (SMMs). Past two decades have also witnessed the enormous growth in the synthesis and magnetic characterization of coordination aggregates (CAs) based on only *4f* ions and *3d-4f* ions together for exciting molecular structures and potential to exhibit SMM behavior. Such studies lead to the consideration that in such CAs a high spin ground state (S) and a negative magnetic anisotropy (D) must be present to attain high anisotropic energy barriers (U_{eff}) for the reversal of magnetization.[2] Such molecule-based nano-magnets thus have received considerable interest because they present themselves as discrete models for understanding the quantum phenomenon and varied applications in the fields of quantum computing,[3] spintronics,[4] and high density information storage.[5] Till to date many such SMMs bearing *3d*, *3d−4f*, or *4f* ions have been obtained with the aim of increasing the blocking temperature (T_B).[6-8] Most of the *4f* ion based systems have better performance, compared to pure *3d*-based SMMs, due to strong magnetic anisotropy of *4f* ions. Which arises from the combination of large magnetic moments, strong spin–orbit coupling and crystal-field effects.[9]

Only recently 4f ion bearing mononuclear SMMs have reached an operational temperature above 77 K.[10] However, *4f* ions show weak magnetic coupling when present at the adjoining coordination sites and bridged by one of more donor atoms.[11] As a result considerable synthetic challenges have been taken for the construction of new genre of *3d−4f* coordination aggregates which can increase the strength of magnetic coupling and suppression of quantum tunneling of magnetization (QTM).[12] Depending upon the design characteristics to convey efficiently the coupling effect of different paramagnetic centers in SMMs, it has been observed that the selected multitopic ligands do participate efficiently in trapping multiple number of *3d* and *4f* ions to grow multinuclear CAs. Choice and efficacy of these ligands

depend on the nature of coordination sites and its back bone to bring the two types of metal ions in close proximity. Recent synthesis, structure determination and theoretical modeling studies have shown that the height of the magnetization relaxation barrier depends on both single-ion anisotropy and *3d-4f* magnetic exchange interactions. As a result, when the *3d-4f* magnetic exchange coupling is adequate, the exchange-coupled levels are well separated (avoiding mixing of low-lying excited states in the ground state) and suppression of QTM is observed. This results in the observation of large energy barriers, hysteresis loops and relaxation. Thus, magnetic interactions between the *3d* and *4f* ions bound to a new ligand anion platform can be effectively utilized to slow down the magnetic relaxation process.

Phenol-based Schiff base derivatives having one or more alcohol arms are versatile ligands for the synthesis of variety of *3d-4f* coordination compounds. Such ligand anions are well suited to grow *3d-4f* aggregates, wherein the imine donor site can bind *3d* ion and the phenolate ion bridge the *3d* and *4f* ions. Combination of these donor sites along with alcohol ends can bind several *3d* and *4f* ions to exhibit the magnetism arising from the contributions of large local magnetic anisotropy and favorable magnetic exchange coupling.[13] Multimetallic complexes containing nickel(II) and lanthanide(III) ions are of interest because of the dominant ferromagnetic exchange interactions observed frequently.[14] Up till now, many Ni–Ln based complexes of varying nuclearity have shown magnetic behavior necessary for magnetic refrigeration.[15] For some time we have been working in controlling the assembly of multiple *3d* ions in CAs to study their spectroscopic, magnetic, catalytic and functional properties.[16]

Herein we report a new family of Ni_4Ln_4 complexes (Ln = Gd, **1**; Tb, **2**; Dy, **3**; Ho, **4**; Yb, **5**) assembled from two symmetric Ni_2Ln_2 cubes, using 2-[{(2-hydroxypropyl)imino}methyl]-6-methoxyphenol (H_2L) ligand (Chart 1). Initial growth of heterometallic and distorted Ni_2Ln_2 cubes are achieved on μ_3-supports from ligand phenoxido and ancillary hydroxido groups.[17] Demand for higher coordination number of the lanthanide(III) ions and preference for bigger coordination spheres permitted the final connections of two such cubes around the Ln^{III} centers by four AcO^- and two HO^- bridges (Chart 2). The synthesis, characterization and magnetic behavior of a new family of Ni-Ln aggregates are discussed.

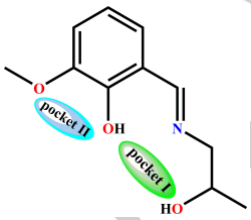

Chart 1. H_2L used in this work.

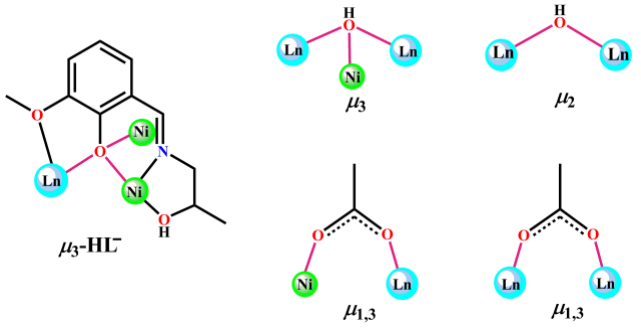

Chart 2. Coordination modes of HL^-, OH^- and OAc^- observed in this work.

Results and Discussion

Synthetic Aspects. The formation of complexes **1–5** resulted from sequential reaction of $Ln(NO_3)_3{\cdot}nH_2O$ (n = 6 or 5) (Ln = Gd, Tb, Dy, Ho, Yb) and $Ni(OAc)_2{\cdot}4H_2O$ with H_2L (1:1:1 molar ratio) in MeCN-MeOH medium in presence of LiOH, under standard laboratory and room temperature conditions.

H_2L was obtained from a Schiff base condensation reaction of o-vanillin and 1-amino propan-2-ol. Heterometallic (*3d-4f*) complex forming ability of the anion of H_2L was explored during the reactions with lanthanide(III) and nickel(II) ions in mixed solvent medium followed by room temperature evaporation. Direct crystallizations from the final reaction solution afforded octanuclear complexes **1–5**, suitable for X-ray structure analysis. (eq 1)

$$4H_2L + 4Ln(NO_3)_3{\cdot}(5\text{-}6)H_2O + 4Ni(CH_3COO)_2{\cdot}4H_2O + 8LiOH \xrightarrow[(3:1,v/v)]{MeCN:MeOH} [Ni_4Ln_4(\mu\text{-}HL)_4(\mu_3\text{-}OH)_4(\mu\text{-}OH)_2(\mu\text{-}OOCCH_3)_8]{\cdot}(NO_3)_2{\cdot}(12\text{–}24)H_2O + 8Li^+ + 10NO_3^- + (38\text{–}54)H_2O \quad \ldots\ldots\ldots (1)$$

In situ generated HO^- ions were judiciously utilized for the hydrolytic aggregation of eight metal ions of two discrete types and supported by four μ-HL^- ions. Nickel(II) salt derived all the $CH_3CO_2^-$ ion were quantitatively consumed for the intra- and inter-cubic connections within the molecular aggregates. No externally added CH_3CO_2Na salt was necessary for the eight $CH_3CO_2^-$ ions utilized in **1–5**.

Initial characterizations of the CAs in the solid state were performed from the use of FT-IR (ATR technique) spectroscopy and PXRD studies. These data are useful for the quantification and characterization of the powder samples obtained after each synthesis. The PXRD patterns of the synthesized samples are in good agreement with the simulated ones from the single-crystal XRD data for each complex. Earlier Mutka et al. and Liu et al have shown that corresponding phenol-based ligands are useful with nickel salts to provide Ni_4O_4 cube structures.[18a,18b] Thereafter the ligands with modified side arms are further explored by many groups for 3d-4f aggregate formation. The anionic form of 2-(benzothiazol-2-ylhydrazonomethyl)-6-methoxyphenol (H_2L) on reaction with $Ni(OAc)_2{\cdot}4H_2O$ and $Ln(ClO_4)_3{\cdot}6H_2O$ provides $[Ni_2Ln_2(\mu_3\text{-}OH)_2(OH)(OAc)_4(HL)_2(MeOH)_3](ClO_4){\cdot}3MeOH$ (Ln = Dy, Tb and Gd) with several terminally bound HO^-, AcO^- and MeOH groups as reported by Liu et al.[19] Tong et al. shown that room temperature single pot reaction of o-vanillin, 2-hydrazinopyridine, $Ni(ClO_4)_2{\cdot}6H_2O$ and $Ln(OAc)_3{\cdot}6H_2O$ in MeOH-EtOH gave $[Ni_2Ln_2(\mu_3\text{-}OH)_2(L)_2(OAc)_4(H_2O)_{3.5}](ClO_4)_2{\cdot}3H_2O$ having terminal coordination of AcO^-, EtOH and H_2O inhibiting further aggregation.[17b] Hor et al. reported a Ni_3Ln type cubane type complex from the use of 2-(hydroxymethyl)pyridine as ligand, $Ni(OAc)_2{\cdot}4H_2O$ and $Ln(OAc)_3$ in THF medium (Scheme 1).[20] In our work we are fortunate enough to obtain further aggregation

from two initially formed Ni_2Ln_2 cubes and new bridging connections of four AcO^- and two HO^- groups. Thus, the nature of ligand system and the choice of synthetic protocol are deterministic for the new routes for octanulcear *3d-4f* coordination aggregates.

To identify the structural integrity of the aggregates in solution, HRMS analysis was used in MeOH solutions. The mass spectra identify a mononuclear ligand anion bound Ni^{2+} fragment $[Ni(HL)]^+$ at a m/z value of 266.05 (calcd. 266.03 for $C_{11}H_{14}NNiO_3$) and two prominent peaks at *m/z* of 475.17 (calcd. 475.13 for $C_{22}H_{29}N_2NiO_6$) and 531.09 (calcd. 531.05 for $C_{22}H_{27}N_2Ni_2O_6$) which were assignable to the fragments of $[Ni(HL)(H_2L)]^+$ and $[Ni_2(L)(HL)]^+$ respectively. (Figure S7 and S8) However, we are unable to detect any peak corresponding to lanthanide bound fragments.

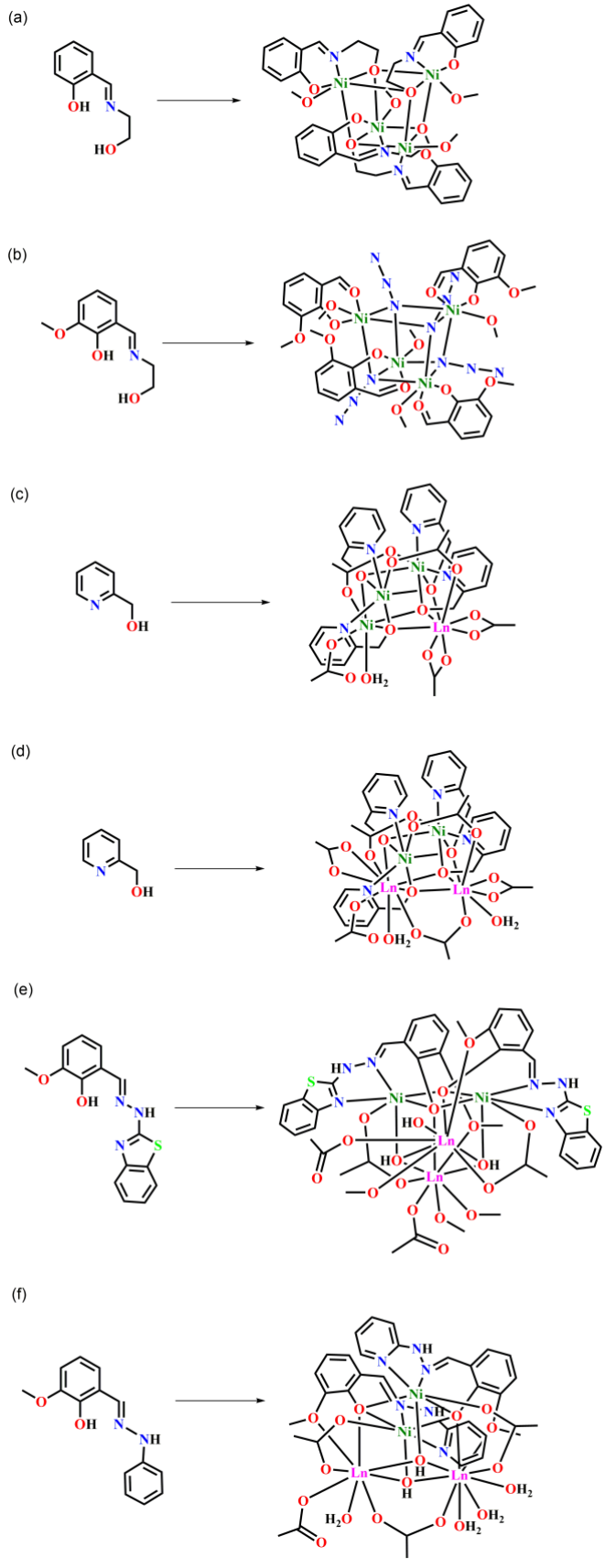

Scheme 1. Some previously known examples of cubes by allied ligands with Ni only (a),[18a] (b)[18b] and Ni-4f metals (c),[20] (d)[17a], (e)[19] and (f)[17b]

Initial Solid State Characterizations

The solid products obtained from the above reactions as crystalline material were first checked by recording their ATR-FT-IR signatures, DRS bands and PXRD patterns.

FT-IR spectra

The FT-IR spectra of complexes **1–5** are similar, showing the representative $\tilde{\nu}_{C=N}$ stretching frequency in 1651-1655 cm^{-1} range for positively charged metal ion bound imine groups. For the free H_2L the corresponding $\tilde{\nu}_{C=N}$ stretching vibration is observed at 1631 cm^{-1} (Figure S1 in SI). The presence of bridging HO^- groups and lattice water molecules are revealed by one broad band within 3415–3362 cm^{-1}. For the complexes **1**–**5**, the asymmetric carboxylate stretching vibrations, $\tilde{\nu}_{as(COO)}$, are found at 1565, 1567, 1569, 1567 and 1560 cm^{-1}, while the symmetric ones for $\tilde{\nu}_{s(COO)}$ appear at 1411, 1417, 1424, 1416 and 1411 cm^{-1}, respectively. The calculated differences $\Delta\tilde{\nu}$ ($\tilde{\nu}_{as(COO)} - \tilde{\nu}_{s(COO)}$) for each complex remain within 149-154 cm^{-1}, confirming the presence of $\mu_{1,3}$-carboxylato bridges at the two Ni···Ln faces of each cube and two other for connecting two such Ni_2Ln_2 cubes from the Ln^{III} corners of the cubes.

Powder X-ray diffraction

The powder and crystalline compounds from different synthetic attempts were characterized using the powder XRD patterns taken in Bruker AXS Powder X-ray diffractometer for complexes **1**–**5**. The experimentally obtained patterns were then compared with the simulated ones found from the single-crystal X-ray diffraction data. In all cases the as obtained experimental patterns show good agreement with the simulated ones (Figure S4 in SI). The slight differences in intensity in some 2θ values are due to the different orientations of the powder crystallites. From the similarity patterns thus obtained, we can conclude that the powder samples available from different batches of synthesis are phase pure and have the same composition to that of the single crystals grown from the solution medium.

Electronic Spectra

The solid state diffuse reflectance spectra (DRS) in 200-1200 nm range for **1**–**5** are characteristic and representative for their identity in the solid state (Figure S3 in SI). The characteristic peaks for ligand field transitions for distorted octahedral Ni^{II} centers in these aggregates are identified with certainty. The five low energy broad absorption bands at 987, 982, 987, 978 and 989 nm can be assigned for the spin allowed $^3A_{2g}(F) \rightarrow {}^3T_{1g}(F)$ transitions for the five complexes **1**–**5** respectively. The next high energy absorption band for $^3A_{2g}(F) \rightarrow {}^3T_{1g}(P)$ transitions are

observed at 611, 607, 607, 610 and 610 nm respectively. The lowest energy $^3A_{2g}$ (F) → $^3T_{2g}$ (F) transitions are not detected for any of these complexes. Whereas the peaks at 350, 350, 352, 345 and 346 nm are intense and assigne gh evaporative crystallization from LMCT transitions. The intra-ligand π → as intense peaks at 288, 268, 294, 261 and 288 nm respectively for **1**–**5**.

Description of Crystal Structures. X-ray quality block shaped

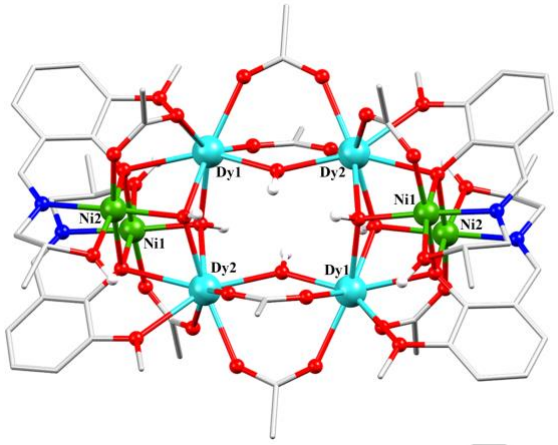

Figure 1. POV-ray presentation of 3 with metal atom numbering scheme. H atoms and counter anions are omitted for clarity. Color code: C, grey; N, blue; O, red; Dy_{III}, cyan; Ni_{II}, green; H, white.

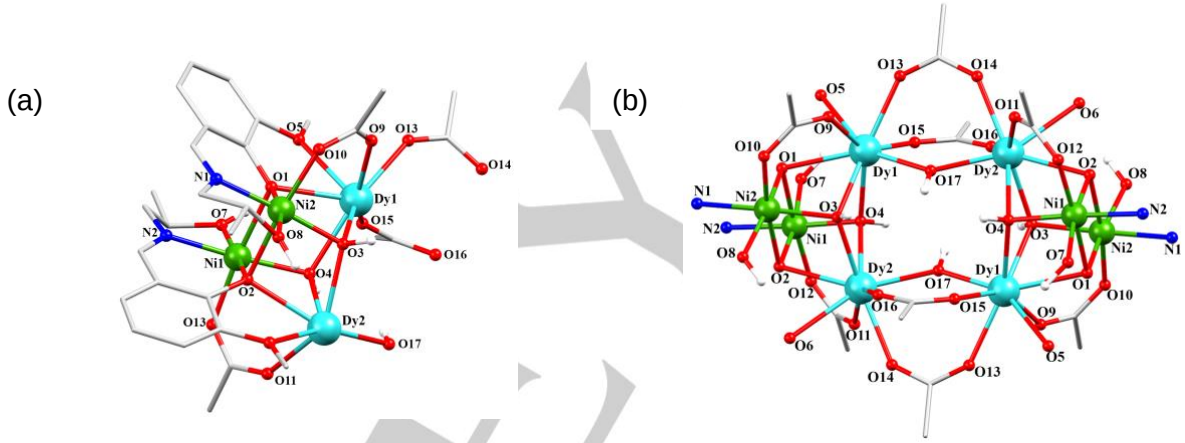

Figure 2. (a) POV-ray presentation of asymmetric unit of 3 and (b) the core structure with atom numbering scheme. H atoms and counter anions are omitted for clarity. Color code as above.

the reaction solutions after 5 days. The detail molecular structures of the complexes **1**–**5** were established from single crystal X-ray structure determinations. All the complexes are isostructural and only differ in the number of water molecules present within the crystal lattices. Complexes **1**, **3** and **4** crystallize in the triclinic *P* $\bar{1}$ space group with Z = 1, whereas **2** and **5** crystallize in the monoclinic *C*2/m space group with Z = 2. The detail discussion is made for the structure of **3** as a representative case to illustrate the common structural features within the family.

$[Ni_4Dy_4(HL)_4(\mu_2\text{-}OH)_2(\mu_3\text{-}OH)_4(\mu\text{-}OOCCH_3)_8](NO_3)_2\cdot 17H_2O$ (3). The molecular structure of **3** showing the triply bridging connectivity from the Dy_{III} sides of two Ni_2Dy_2 cubic units is presented in Figure 1. The details of the crystal data and refinement parameters for **1**−**5** are summarized in Table 1. Selected interatomic separations and bond angles around the metal ion centers are listed in Table S4–S7. The asymmetric unit of **3** consists of a single Ni_2Dy_2 cubic core formed from two HL^- units, two Dy_{III} ions, two Ni_{II} ions, four AcO^- ions and three HO^- groups (Figure 2a). Two AcO^- and one HO^- ions are utilized to develop the separated double cubane Ni_4Dy_4 structure (Figure 2b). The whole structure of **3** revealed a dicationic complex, $[Ni_4Dy_4(HL)_4(\mu_3\text{-}OH)_4(\mu_2\text{-}OH)_2(\mu\text{-}OOCCH_3)_8]^{2+}$, associated with two NO_3^- ions available from the nitrate salt of Dy_{III} and seventeen water of crystallization. Interestingly, the four AcO^- ions originating from the Ni_{II} salt and two HO^- ions from LiOH are consumed in stoichiometric amounts to establish the inter-tetramer bridges. Other AcO^- and HO^- bridges are utilized to sustain the individual cubic Ni_2Dy_2 units. The tridentate ONO pocket from one HL^- showed *meridional* binding to one Ni_{II} center. Whereas the adjacent bidentate OO pocket is chosen to trap the hard, bigger and *oxophilic* Dy_{III} center already attached to several H_2O molecules in the reaction medium. De-protonation of one such H_2O molecule provided Dy_{III} bound HO^- ion suitable to embrace the ligand anion bound entity as $\{NiDy(HL)(OH)(OAc)(H_2O)_n\}$. Two phenoxido donors from two HL^- bridge two Ni_{II} centers to give the Ni_2O_2 face while two HO^- ions bridge two Dy_{III} ions for Dy_2O_2 face.

Dy1 and Dy2 are double-bridged by two μ_3-O atoms from two HO^- groups whose third arm is extended to Ni1 and Ni2 and thus form the Dy_2O_2 rhombus face. The Ni_2O_2 faces register O–Ni–O angles ranging from 81.65(12)° to 81.72(12)°. Formation of two such Dy_2O_2 open faces is important to establish the inter-cubic

connections for separated double-cubane arrangement. Two HL^- units are involved in binding and assembling of one cubic Ni_2Ln_2 sub-unit. Each MeO− arm of the ligand anion (HL^-) is engaged in terminal coordination to Dy^{III} ions selectively and thus the central phenoxido group is allowed to bridge two other Ni^{II} ions. From the HL^- anions the available PhO^- and the adjacent −OMe function made the bidentate O,O chelation available to Dy^{III} centers providing narrow O1–Dy1–O5 angle of 60.67(11)° and O2–Dy2–O6 angle of 61.17(10)°. The Ni···Ni

Table 1. Crystal data and refinement parameters for complexes **1–5.**

	1(Ln=Gd)	**2(Ln=Tb)**	**3(Ln=Dy)**	**4(Ln=Ho)**	**5 (Ln=Yb)**
Empirical formula	$C_{60}H_{90}Gd_4N_6Ni_4O_{42}$	$C_{60}H_{90}Tb_4N_6Ni_4O_{42}$	$C_{60}H_{90}Dy_4N_6Ni_4O_{42}$	$C_{60}H_{90}Ho_4N_6Ni_4O_{42}$	$C_{60}H_{90}Yb_4N_6Ni_4O_{42}$
Formula weight	2431.21	2437.89	2452.21	2461.93	2494.34
Crystal system	Triclinic	Monoclinic	Triclinic	Triclinic	Monoclinic
Space group	$P\bar{1}$	*C*2/m	$P\bar{1}$	$P\bar{1}$	*C*2/m
a (Å)	12.9729(8)	16.631(7)	13.152(11)	12.9782(10)	16.67(3)
b (Å)	14.6039(9)	28.317(6)	14.926(9)	14.6759(11)	28.06(6)
c (Å)	15.2051(10)	17.244(5)	15.426(8)	15.2575(11)	17.27(3)
α (°)	113.636(2)	90	113.794(10)	114.549(2)	90
β (°)	111.059(2)	141.891(15)	110.409(16)	111.040(2)	142.67(2)
γ (°)	93.730(2)	90	94.62(3)	93.334(2)	90
Volume ($Å_3$)	2388.0(3)	5012(3)	2509(3)	2392.4(3)	4901(16)
Z	1	2	1	1	2
D_{calcd} (g cm^{-3})	1.691	1.615	1.623	1.709	1.688
Absorption coefficient (mm^{-1})	3.589	3.596	3.751	4.118	4.608
F (000)	1196	2400	1204	1208	2432
Temperature/K	196.15	180.0	196.96	196(2)	150.0
Reflections collected/unique	34041 / 12924	24267 / 5694	23805 / 11347	28710 / 8530	23061 / 5617
Parameters	573	292	537	534	287
limiting indices	−16 ≤ h ≤ 18, −20 ≤ k ≤ 20, −20 ≤ l ≤ 22	−21 ≤ h ≤ 20, −36 ≤ k ≤ 31, −19 ≤ l ≤ 22	−16 ≤ h ≤ 17, −19 ≤ k ≤ 12, −20 ≤ l ≤ 20	−15 ≤ h ≤ 15, −17 ≤ k ≤ 17, −18 ≤ l ≤ 18	−21 ≤ h ≤ 21, −35 ≤ k ≤ 36, −22 ≤ l ≤ 22
Goodness-of-fit (F_2)	1.036	1.088	1.062	1.031	1.041
Largest diff peak/ hole (e $Å_{-3}$)	3.914, -2.443	1.803, -1.082	1.706, -3.226	1.918, -1.191	2.831, -1.608
R_{int}	0.0288	0.0377	0.0451	0.0515	0.0765
R1; wR2 [I >2σ(I)]	0.0477; 0.1385	0.0329; 0.0707	0.0435; 0.1180	0.0361; 0.0867	0.0403; 0.0926
CCDC	1989262	1989264	1989261	1989265	1989263

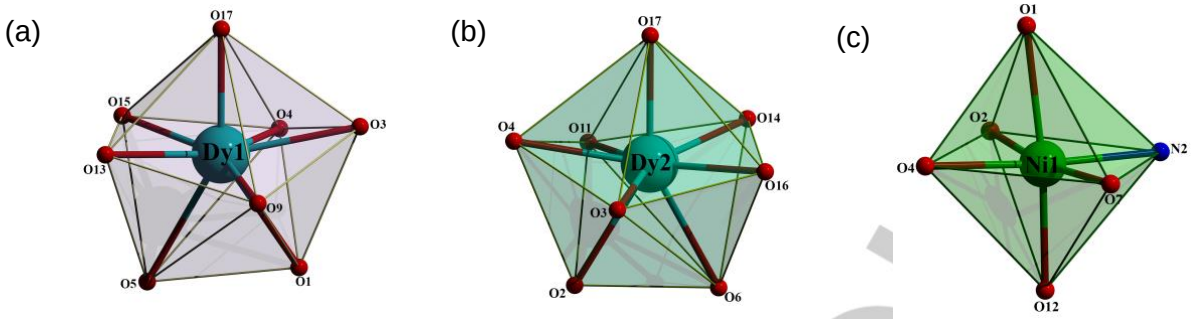

Figure 3. (a) and (b) Distorted trigonal dodecahedral coordination environment around the $Dy1_{III}$ and $Dy2_{III}$ center; (c) Distorted octahedral coordination environment around the Ni_{II} center. Color code: O, red; N, blue; Dy_{III}, cyan; Ni_{II}, green.

separation within each Ni_2Dy_2 cube structure is shortest at 3.245 Å. The Dy1···Dy2 separation is longest (3.929 Å) at the Dy_2O_2 rhombus face. Coordination of two imine N donors from HL^- are utilized to bind two Ni_{II} centers giving normal Ni–N distances of 2.009(4) and 2.015(4) Å. The O donors from the alcohol OH arms showed chelation with slightly longer Ni–O(H) bonds of 2.088(4) Å and 2.095(4) Å. Two AcO^- ions in $\mu_{1,3}$ mode span two Ni···Dy faces providing Ni1···Dy2 and Ni2···Dy1 separations of 3.420 Å and 3.432 Å respectively, which are of intermediate type. Two other Ni···Dy faces, devoid of acetato-bridges register higher magnitude of Ni···Dy separations at 3.579 Å and 3.557 Å for Ni1···Dy1 and Ni2···Dy2 respectively. The bigger Dy_{III} centers at the two corners of each cube thus have vacant coordination sites to attract other donors. One Dy_{III} from each cube thus binds two AcO^- and one HO^- units and link another Dy_{III} center of Dy_2O_2 face of adjacent cube. Two such $(AcO)_2(HO)$ bridges are thus utilized to connect two Ni_2Dy_2 cubes registering long inter-tetramer Dy···Dy separation of 4.145 Å (Dy1···Dy2) (Figure 4). The crystal packing diagram reveals the shortest Dy···Dy distance between neighboring molecule is 9.730 Å (Figure S6).

Within the octameric structure all four Ni_{II} centers remain in distorted octahedral O_5N coordination geometry (Figure 3b) as verified from Continuous Shape Measures (CShM) by using SHAPE 2.1[21] (Table S3). Amongst the five oxygen donors, two are from phenoxido group, one each from ligand alcohol arm and bridging hydroxido group, and the fifth one from acetato group. The Ni–O distances vary within 2.004(3)–2.262(3) Å, in which the shortest one is found for hydroxido oxygen (Ni2–O3) and longest one for phenoxido oxygen (Ni2–O2). The extent of distortion from the ideal octahedral geometry is detected from the narrower O–Ni–O adjacent angles of 80.37(12) and 81.34(12)°, and opposite O–Ni–O angles of 173.38(12) and 174.68(13)°. The O_8 coordination geometry around each Dy_{III} center is distorted trigonal dodecahedral (Figure 3a) one as verified from CShM (Table S2). The trigonal dodecahedral coordination geometry around the four bigger Dy_{III} ions forces a distortion around the coordination environment of adjacent Ni_{II} ions. The eight O donors are assembled from one ligand PhO^- (Dy1–O1, 2.474(3) Å; Dy2–O2, 2.456(3) Å), one ligand −OMe group (Dy1–O5, 2.597(3); Dy2–O6, 2.593(4) Å), two μ_3-HO^- (Dy–O, 2.369(3)–2.437(3) Å), one μ_2-HO^- (Dy1–O17, 2.260(3); Dy2–O17, 2.258(4) Å) and three bridging acetato (Dy–O, 2.338(4)–2.373(4) Å) groups. The ligand derived −OMe functions around each Dy_{III} ions thus record the longest Dy−O bonds. The oxygen atoms from μ_3-HO^- donors (O3, O4) provide O−Dy−O angles of 67.09(11)° and 66.61(11)°. Other O−Dy−O angles vary within 61.17(10)° to 151.50(11)°. The μ_3 bridging nature of HO^- groups (O3 and O4) at the corners of the cube record Dy1−O3−Dy2 and Dy1−O4−Dy2 angles of109.48(12)° and 109.66(12)° respectively, which are away from angles close to 90° commonly observed for isolated Ni_4O_4 type cube structures.[22] The Dy1−O3−Ni2, Dy2−O3−Ni2, Dy1−O4−Ni1 and Dy2−O4−Ni1 angle on the other hand span from 99.69(13)° to 108.88(14)°. Lengthening of bonds at the shared μ_3 type HO^- and PhO^- bridge heads, due to presence of Dy_{III} ions ultimately lead to distortion around the adjacent Ni_{II} ions.

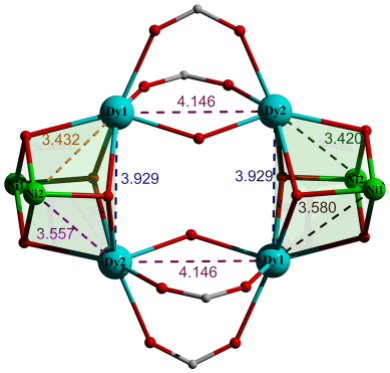

Figure 4. Metallic core view of complex **3** showing intermetallic separations

Discussion of magnetic properties

Magnetic susceptibility data for the complexes **1**–**5** were collected at 200 Oe (2-30 K) and 3000 Oe (2-300 K). The temperature dependence plot of χT at 2-300 K are shown in Figure 5. The relevant susceptibility and saturation magnetization data for all complexes are collected in Table 2.

The χT values at 300 K are in agreement with the expected theoretical values for four Ni_{II} (S =1, g = 2.0) and four Ln_{III} ions, taking into account the spin-only moment for complex **1** or strong spin-orbit coupling for complexes **2**–**5**. The χT products are mostly constant down to 100K, between 100 K and 30 K there is a slight decrease in χT for all except **1** and below 30 K an increase is observed in all cases. The low temperature increase indicates ferromagnetic interactions between the metal ions that from complexes **1** to **5**, this increase is field dependent. A slight decrease in χT observed for **2**–**5** between 100 K and 30

Table 2. Comparison of calculated and experimental χT data

Complexes	χT (300 K, cm^3 K mol^{-1})	Expected χT (300 K, cm^3 K mol^{-1})	Ni(II), S = 1, g = 2.0	M//NAμB (2 K)
1	34.13	35.6	$^8S_{7/2}$, S = 7/2, L = 0, g = 2.0	33.00
2	46.48	51.24	$^7F_6$, S = 3, L = 3, J=6 and g_J= 3/2	22.82
3	55.65	60.64	$^6H_{15/2}$, S = 5/2, L = 5, J=15/2 and g_J= 4/3	26.41
4	54.36	60	$^5I_8$, S = 2, L = 6, J=8 and g_J= 10/8	27.13
5	13.53	14	$^2F_{7/2}$, S = 1/2, L = 3, J=7/2 and g_J= 1.19	13.03

K can be attributed to the depopulation of M_J sublevels of the lanthanoid ion.

The crystal structures of the complexes show the linking of two Ni_2Ln_2 cubanes by four AcO^- and HO^- ancillary bridges as shown in Scheme 2. In each cubane part the Ni–O–Ni angles are 98.06(15)° and 98.84(16)°, 98.0(2)° and 98.00(2)°, 98.80(12)° and 97.82(12)°, 98.67(16)° and 97.89(15)°, and 95.70(3)° and 96.00(3)° for complexes **1**–**5** respectively. The Ni–O–Ln angles on the other hand are between 97.68° and 108.85° and Ln–O–Ln angles remain between 108.97° to 111.75° for the all the five complexes. The Ni···Ni exchange coupling is expected to be ferromagnetic in nature for Ni–O–Ni angles of 98° or less but when the Ni–O–Ni angle is 98° or more, the coupling can be antiferromagnetic in nature.[23] The coupling between Ni^{II} and Ln^{III} can be either ferromagnetic or antiferromagnetic, but as usual the 3d-4f coupling is very weak.[7a,24] Each Ni_2Ln_2 unit is linked to another one forming a octamer through the Ln_2O_2 face of each cubane part. The Ln–Ln distance is quite long, 4.107 Å–4.145 Å for complexes **1**–**5**, thus the coupling between Ni_2Ln_2 units will be in turn very weak.

Magnetization vs. field plots at 2 K are shown in Figure 6. They clearly show for all species the population of a magnetic ground state, consistent with the existence of some component of ferromagnetic coupling in the complexes. The susceptibility and magnetization data for **1** was fitted using the software PHI.[25] The model was a simple Ni_2Ln_2 unit with intermolecular interactions included as zJ' exchange. The program was designed for the treatment of systems containing orbitally degenerate and strongly anisotropic ions, through the inclusion of a full Hamiltonian with Exchange, Zeeman, Spin-orbit coupling and Crystal Field effects, as shown in Equation 2. In our simple model, crystal field effects on the Ni^{II} were not included to avoid overparameterization and g was fixed as 2.0 for all ions. Equation 3 shows the full exchange Hamiltonian used in PHI.

$$\hat{H} = \hat{H}_{SO} + \hat{H}_{EX} + \hat{H}_{CF} + \hat{H}_{ZEE} \quad \text{.....(2)}$$

$$\hat{H}_{EX} = -2 \sum_{i<j}^{i,j \in N} \hat{\vec{S}}_i \cdot \overline{\overline{J_{ij}}} \cdot \hat{\vec{S}}_j = \hat{H}_{(an)iso} + \hat{H}_{anti} \quad \text{.....(3)}$$

The best fit was obtained for J_1(Ni–Ni) = -0.767 cm^{-1}, J_2(Gd–Gd) = 0.144 cm^{-1} and J_3(Ni–Gd) = -0.037 cm^{-1}. As expected, the inter-Ni_2Gd_2 unit is the smallest, with a value of J(Ni_2Gd_2–Ni_2Gd_2) = zJ' = 0.0013 cm^{-1}. The exchange couplings are all small, as expected and J(Ni–Ni) is antiferromagnetic, in agreement with the exchange values tabulated for various other Ni^{II} cubanes with Ni–O–Ni angles of 98° or larger. The Gd–Gd exchange coupling is according to the fitting small but ferromagnetic while the Ni–Gd coupling is small and antiferromagnetic. In the structure Ni–O–Ln angles are 97.67° to 99.23° and Ni–OH–Ln are between 99.68° and 108.29°, while there is also a syn,syn- carboxylato bridge. With these structural parameters, weak ferromagnetic coupling should be expected for adjacent Ln–Ni centers mediated by the monoatomic oxygen bridges while an antiferromagnetic contribution is expected for the syn,syn-carboxylato pathway. This result in a very small, near zero exchange coupling between Ni–Gd, as calculated by the best fit. We can compare this complex with our previously

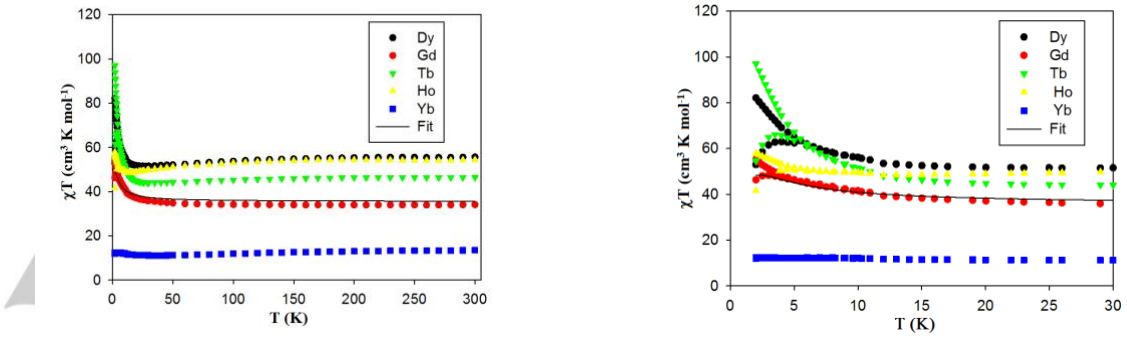

Figure 5. Temperature dependence susceptibility (χT) data for complexes **1**–**5** measured with a dc field of 3000 Oe (left), and the low temperature region with a dc field of 198 Oe for clarity (right). The solid black line is a fit of the experimental data for complex **1**.

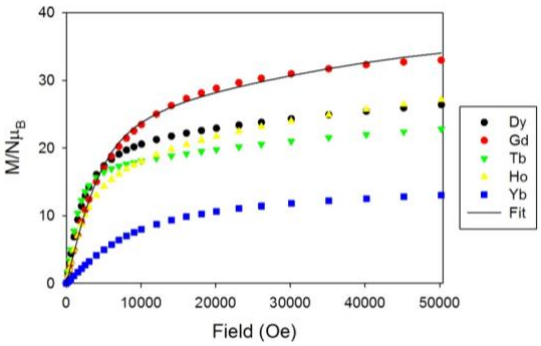

Figure 6. Field dependence of magnetization for complexes **1**−**5** at 2 K.

reported Ni_2Gd_2 cubane.[26] In those cubanes we observed very weak ferromagnetic Gd–Gd and Ni–Gd interactions. The exchange constants are very similar, obtained with the same fitting software, to the ones reported here, but the small distortions imposed by the aggregation of the cubanes into a Ni_4Ln_4 unit can be responsible for the small differences observed, in particular the Ni-Gd exchange constant. The main distortion is the Ln–Ln separation in Ni_4Ln_4 (3.91 Å for Ni_4Gd_4 complex vs 3.78 Å for Ni_2Gd_2). The exchange values result in an S = 14 spin ground state for **1**(Gd), due to the weak ferromagnetic coupling between two Ni_2Gd_2 units. However, due to the combination of weak exchange both ferromagnetic and antiferromagnetic there is some degree of frustration in the system and the ground state is not isolated from several excited states that span a few cm^{-1} in energy.

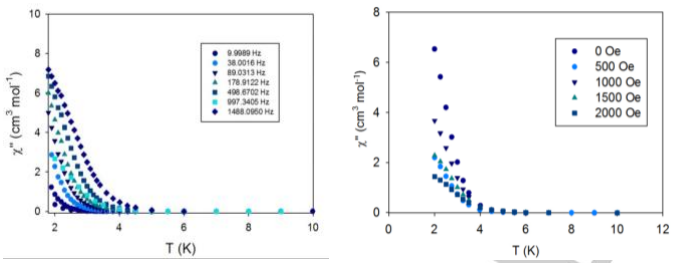

Figure 7. Out-of-phase ac magnetic susceptibility for **3** without applied dc field at the indicated frequencies (left) and at the indicated dc fields (right).

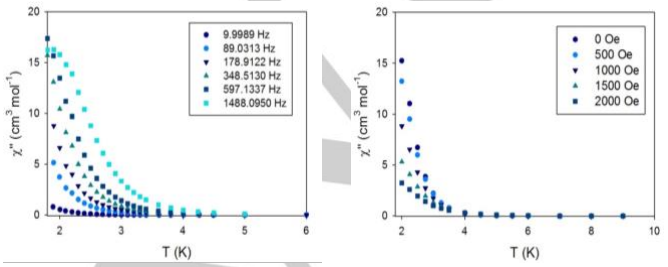

Figure 8. Out-of-phase ac magnetic susceptibility for **2** without applied dc field at the indicated frequencies (left) and at the indicated dc fields (right).

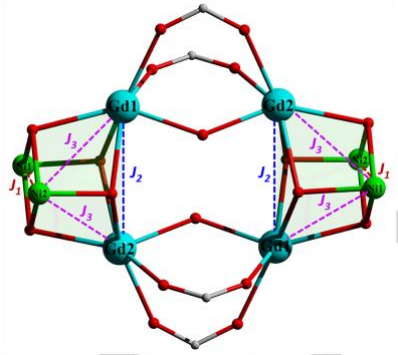

Scheme 2. Magnetic coupling interactions in complex **1**. Ni_{III} green, Ln_{III} cyan.

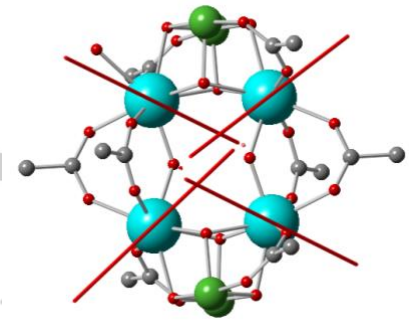

Figure 9. Views of the orientation of the anisotropy axes on the Dy_{III} ions of Ni_4Dy_4, calculated by Magellan and depicted as red solid lines.

The dynamics of magnetization relaxation for these complexes was studied by ac magnetic susceptibility and are shown in Figure 7 and Figure 8. Only **2** and **3** showed tails of peak in the out-of-phase ac magnetic susceptibility when no dc field was applied during the measurement. Both **2** and **3** are SMMs with low blocking temperatures typical of 3d-4f SMMs. For **3**, the peak is not fully observed if a dc field is applied. The results are similar for **2**. This indicates fast relaxation for these complexes, probably due to QTM. Neither of the other complexes is an SMM.

The fitting of the susceptibility and magnetization data for **1** indicated that the anisotropy of the four Ni_{II} ions was not a key parameter in the magnetic properties. This has been observed before while comparing analogous Ni_{II} and Co_{II} complexes.[27] Thus, only for the most anisotropic lanthanide ions Dy_{III} and Tb_{III} the SMM behavior are observed. Since only the tail of an out-of-phase peak is observed down to 2 K, this indicates that relaxation of the magnetization is still fast at these low temperatures for both **2** and **3**.

The software Magellan[28] has been used to calculate the orientation of the anisotropy axes on the Dy_{III} ions of the Dy analogue **3**. The software uses a purely electrostatic model for the calculation. As can be observed in Figure 9, the anisotropy axes on the two Dy of each Ni_2Dy_2 cubane are not oriented parallel to each other, in fact they are at a 43º angle. This results in small molecular anisotropy, and thus it agrees well with observed dynamic properties of **3**: that is the absence of a large energy barrier for the relaxation of the magnetization. Furthermore, one can compare the coordination polyhedra around the Tb_{III} and Dy_{III} ions, shown in Figure 3. Clearly, the distorted geometry observed does not agree with a sandwich-like distribution of the ligands.[29]

Using the same simple prediction Yb should display SMM properties with this equatorial ligand arrangement, but the low spin ground state and the lack of ferromagnetic interactions precludes the observation of SMM properties in the Yb analogue **5**. There are few polynuclear SMMs reported with Yb, since the Yb···Yb coupling is extremely weak.[30]

Conclusion

Coordinating self-aggregation reactions of H_2L and base with $Ni(OAc)_2{\cdot}4H_2O$ and nitrate salts of five lanthanide(III) ions show results for a unique type of self-assembly for selected 3d and 4f block metal ions. Isolation of five Ni_4Ln_4 aggregates is achieved by bridging two Ni_2Ln_2 units, grown on ligand support, by four AcO^- and two HO^- groups giving two new Ln_2O_2 faces. The aggregation process is driven by the higher coordination demand of 4f ions attached to the HL^- through bidentate O,OMe part. These coordination positions are not fulfilled by terminal coordination of solvent and/or water molecules to inhibit the formation of octanuclear entities. The choice of LiOH as base is optimum for the generation of HL^-. *In situ* generation, entrapment and bridging by six HO^- groups controls the formation of octanuclear complexes in chosen reaction condition. Thus *in situ* generation and ready availability of HL^- bound $Ln(OH)_n$ species is central for incorporation of four each 3d and 4f ions in the resulting products. Use of $Ni(OAc)_2$ provides AcO^- ions for face clipping of individual Ni_2Ln_2 cubes as well as in inter-cube connections from the Ln^{III} vertices and establishment of the 3d···4f and 4f···4f links. These two types of networking anions have been exploited to control the particular type of molecular topology within the final products. The variable temperature magnetization measurements indicate a small ferromagnetic interaction for all the complexes. Complexes **2** and **3** show a tail in frequency-dependent out-of-phase ac signal without applied dc field. In this example we succeed in getting a small ferromagnetic $Ni_2Ln_2{\cdots}Ln_2Ni_2$ interaction and two new Ni_4Tb_4 (**2**) and Ni_4Dy_4 (**3**) SMMs with appropriate ferromagnetic coupling. In general, the reported work supplemented the octanuclear family of Ni^{II}-Ln^{III} SMMs and added sensible approaches to the syntheses and isolation of 3d−4f SMMs having new structures and important magnetic properties.

Experimental Section

Materials and Reagents. All the chemicals and reagents used in this work were obtained from the commercial houses and used directly without any further purification. The typical sources were nickel acetate from Loba Chemie, India, and different lanthanide nitrates, 1-amino-2-propanol from Alfa Aesar, India. o-vanillin was obtained from Spectrochem Pvt. Ltd., India and used as received. MeOH and MeCN were reagent grade and obtained from Finar Ltd., India.

Ligand Synthesis. The Schiff base 2-[{(2-hydroxypropyl)imino}methyl]-6-methoxyphenol (H_2L) was prepared *in situ* from a one-step condensation reaction of o-vanillin and 1-amino-2-propanol in a 1:1 molar ratio in MeOH under refluxing condition, as reported earlier.[31] The obtained solution of H_2L was then directly used without isolation and further purification for the different synthesis using different combinations of *3d* and *4f* ions.

General Synthetic Procedure for Complexes 1−5. All the five complexes were prepared from the typical reactions of H_2L with the nickel(II) and lanthanide(III) salts in the presence of stoichiometric amount of LiOH base in a mixed solvent media (Scheme 3). To a MeCN-MeOH (3:1) solution of H_2L (0.1mmol) solid $Ln(NO_3){\cdot}nH_2O$ (0.1mmol) was added under stirring condition to obtain a light yellow solution. After 10 min of stirring, solid LiOH (0.2mmol) was added and the solution was stirred for 1 h. To this another MeOH solution of $Ni(CH_3COO)_2{\cdot}4H_2O$ (0.1 mmol) was added and the whole mixture was further stirred for 7 h period to obtain a green solution, which was next filtered and kept for slow evaporation of solvents in air. Green colored block shaped crystals, suitable for X-ray analysis, were separated out from the solution after 5 days. The stoichiometry of the used reagents and the characterization data of each complex (**1**–**5**) are delineated below.

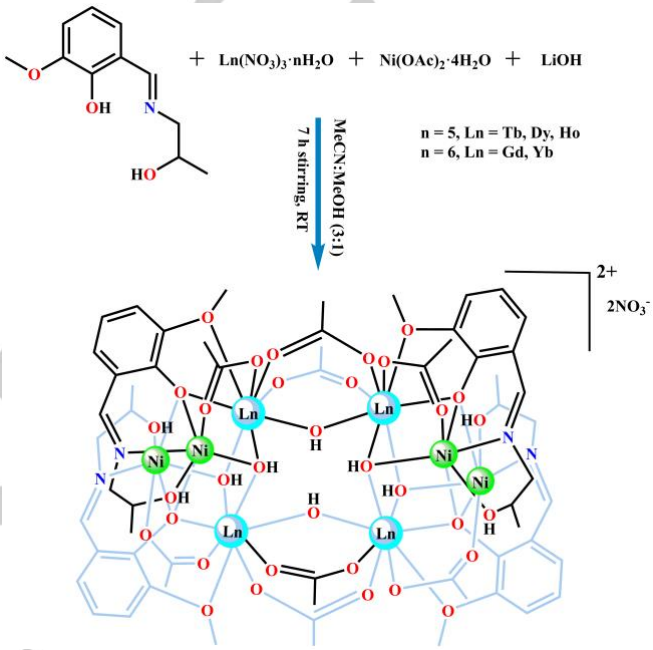

Scheme 3. Syntheses of complexes **1−5**

$[Ni_4Gd_4(HL)_4(\mu_2\text{-}OH)_2(\mu_3\text{-}OH)_4(\mu\text{-}OOCCH_3)_8]{\cdot}(NO_3)_2{\cdot}12H_2O$ (1). H_2L (1mL, 0.1mmol), $Gd(NO_3)_3{\cdot}6H_2O$ (0.0451 g , 0.1 mmol), $Ni(CH_3COO)_2{\cdot}4H_2O$ (0.0260 g, 0.1mmol) and LiOH (0.0840 g, 0.2mmol). Yield: 0.045 g; 75% based on Gd. Anal. Calcd for $C_{60}H_{110}Gd_4Ni_4N_6O_{52}$ (2611.30) C, 27.60; H, 4.25; N, 3.22. Found: C, 27.48 H, 4.14; N; 3.13. Selected FT-IR peaks (KBr, cm^{-1}; s = strong, vs = very strong, m = medium, br = broad): 3377 (br), 1651 (m), 1605 (m), 1565 (s), 1464 (m), 1411 (vs), 1338 (vs), 1264 (s), 1243 (m), 1223 (m), 1078 (m), 1033 (m), 967 (w), 849(w), 750 (m), 643 (m). UV-vis spectra in MeOH: λ_{max}, nm (ε, L mol^{-1} cm^{-1}) 609 (3291), 374 (16369), 278 (33498), 234 (98551), 208 (78138).

$[Ni_4Tb_4(HL)_4(\mu_2\text{-}OH)_2(\mu_3\text{-}OH)_4(\mu\text{-}OOCCH_3)_8]{\cdot}(NO_3)_2{\cdot}24H_2O$ (2). H_2L (1ml, 0.1 mmol), $Tb(NO_3)_3{\cdot}5H_2O$ (0.0435 g, 0.1 mmol), $Ni(CH_3COO)_2{\cdot}4H_2O$ (0.0260 g, 0.1mmol) and LiOH (0.0840 g, 0.2mmol). Yield: 0.041 g. 68% based on Tb. Anal. Calcd for $C_{60}H_{134}Tb_4Ni_4N_6O_{64}$ (2834.19) C, 25.43; H, 4.77; N, 2.97. Found: C, 25.19; H, 4.81; N; 2.89. Selected FT-IR peaks (KBr, cm^{-1}; s = strong, vs = very strong, m = medium, br = broad): 3415 (br), 1654 (m), 1607 (s), 1567 (s), 1465 (m), 1417 (vs), 1342 (s), 1266 (m), 1243 (m), 1225 (m), 1080 (m), 1036 (m), 969 (w), 850 (w), 750 (m), 736 (m),644 (m). UV-vis spectra in MeOH: λ_{max}, nm (ε, L mol^{-1} cm^{-1}) = 603 (2822), 371 (14886), 277 (30626), 233 (88420), 207 (72319).

$[Ni_4Dy_4(HL)_4(\mu_2\text{-}OH)_2(\mu_3\text{-}OH)_4(\mu\text{-}OOCCH_3)_8]{\cdot}(NO_3)_2{\cdot}17H_2O$ (3). H_2L (1ml, 0.1mmol), $Dy(NO_3)_3{\cdot}5H_2O$ (0.0438 g, 0.1mmol), $Ni(CH_3COO)_2{\cdot}4H_2O$ (0.0260 g, 0.1mmol) and LiOH (0.0840 g, 0.2mmol). Yield: 0.038 g; 63% based on Dy. Anal. Calcd for $C_{60}H_{120}Dy_4Ni_4N_6O_{57}$ (2722.38 g): C, 26.47;

H, 4.44; N, 3.09. Found: C, 26.29; H, 4.28, N, 2.93. Selected FT-IR peaks (KBr, cm^{-1}; s = strong, vs = very strong, m = medium, br = broad): 3417 (br), 1654 (m), 1615 (s), 1569 (s), 1467 (m), 1424 (vs), 1335 (s), 1266 (s), 1243 (m), 1227 (m), 1082 (m), 1036 (m), 973 (m), 736 (m), 644 (m). UV-vis spectra in MeOH: λ_{max}, nm (ε, L mol^{-1} cm^{-1}) = 603 (2797), 372 (14330), 278 (29365), 234 (84305), 206 (63638).

$[Ni_4Ho_4(HL)_4(\mu_2\text{-}OH)_2(\mu_3\text{-}OH)_4(\mu\text{-}OOCCH_3)_8]\cdot(NO_3)_2\cdot 19H_2O$ (4). H_2L (1ml, 0.1mmol), $Ho(NO_3)_3\cdot 5H_2O$ (0.0441 g, 0.1mmol), $Ni(CH_3COO)_2\cdot 4H_2O$ (0.0260 g, 0.1mmol) and LiOH (0.0840 g, 0.2mmol). Yield: 0.041 g; 67% based on Ho. Anal. Calcd for. $C_{60}H_{124}Ho_4Ni_4N_6O_{59}$ (2768.13 g): C, 26.03; H, 4.52; N, 3.04. Found: C, 25.82; H, 4.45; N, 3.11. Selected FT-IR peaks (KBr, cm^{-1}; s = strong, vs = very strong, m = medium, br = broad): 3415(br), 1654 (s), 1614 (m), 1567 (m), 1464 (m), 1416 (vs), 1336 (s), 1266 (s), 1243 (m), 1224 (m), 1079 (m), 1034 (m), 968 (m), 737 (m), 644 (m). UV-vis spectra in MeOH: λ_{max}, nm (ε, L mol^{-1} cm^{-1}) = 581 (4265), 373 (14421), 278 (30191), 233 (86648), 206 (67168).

$[Ni_4Yb_4(HL)_4(\mu_2\text{-}OH)_2(\mu_3\text{-}OH)_4(\mu\text{-}OOCCH_3)_8]\cdot(NO_3)_2\cdot 24H_2O$ (5). H_2L (1ml, 0.1mmol), $Yb(NO_3)_3\cdot 6H_2O$ (0.0383 g, 0.1 mmol), $Ni(CH_3COO)_2\cdot 4H_2O$ (0.0260 g, 0.1mmol) and LiOH (0.0840 g, 0. 2 mmol). Yield: 0.042 g. 68% based on Yb. Anal. Calcd for. $C_{60}H_{134}Yb_4Ni_4N_6O_{64}$ (2890.70 g): C, 24.93; H, 4.67; N, 2.91. Found: C, 24.73; H, 4.45; N, 2.74. Selected FT-IR peaks (KBr, cm^{-1}; s = strong, vs = very strong, m = medium, br = broad): 3362 (br), 1655 (s), 1608 (m), 1560 (vs), 1467 (m), 1411 (vs), 1332 (s), 1266 (s), 1243 (m), 1223 (m), 1072 (m), 1036 (m), 963 (m), 737 (m), 648 (m). UV-vis spectra in MeOH: λ_{max}, nm (ε, L mol^{-1} cm^{-1}) = 603 (1702), 372 (13757), 278 (29541), 233 (82353), 207 (61531).

Physical measurements. Elemental analyses (C, H, N) of the complexes were performed on PerkinElmer model 240C elemental analyzer. FT-IR (ATR) spectra were recorded on a PerkinElmer Spectrum Two Spectrometer. Solution phase electronic absorption spectra were recorded using a Shimadzu UV 3100 UV-vis-NIR spectrophotometer. HRMS were recorded in electrospray ionization (ESI) mode using a Bruker esquire 3000 plus mass spectrometer. The solid state diffuse reflectance spectra (DRS) were measured using a Cary model 5000 UV-vis-NIR spectrophotometer. The powder X-ray diffraction (PXRD) patterns were measured on Bruker AXS X-ray diffractrometer using Cu- Kα (λ = 1.5418 Å) radiation source within the angular range of (2θ) 5-50˚ and a fixed-time counting of 4s at 25 °C.

Magnetic measurements. Magnetic susceptibility measurements of polycrystalline complexes **1−5** were performed using quantum Design SQUID MPMS-XL magnetometer equipped with a 5 T magnet in the Unitat de Mesures Magnètiques (Universitat de Barcelona). The dc magnetic susceptibility was measured in the temperature range of 2-300 K using the applied magnetic field of 3000 Oe and below 30 K of 198 Oe. Field-dependent magnetization measurements were performed at 2 K, under the field of 0-5 T. The experimental magnetic data were corrected for the diamagnetism of sample holder and diamagnetic corrections were calculated using Pascal's constants.

X-ray crystallographic measurements. The crystallographic data of the complexes **1−5** were measured on Bruker SMART APEX-II CCD X-ray diffractometer, equipped with a graphite monochromator of Mo-Kα radiation (λ = 0.71073 Å) source. Measurements were performed by using ω scan method at 180-197 K temperature. The software SAINT[32] and XPREP[33] were used for data integration and space group determination. The structures were solved by direct method of SHELXT-2014[34] and refined with full-matrix least squares on F_2 using the SHELXL[35] program package associated with the Olex-2 software.[36] The software SADABS[37] was employed to the data for the absorption correction. The position of heavier atoms (Ni, Ln) were determined easily, and positions of C, N, O were subsequently determined from difference Fourier maps. The atoms were refined anisotropically. The H atoms were placed in calculated positions and refined with fixed geometry and riding thermal parameters with respect to their carrier atoms. The crystallographic diagrams were generated using DIAMOND[38] and POV-ray[39] software. All the complexes **1–5** contain solvent molecules of large thermal parameter and could not be modelled satisfactorily. Hence the solvent molecules were removed by using *PLATON/squeeze*[40] program which generated an electron count of 106, 440, 156, 175 and 452 for complexes **1–5** respectively were assigned for the 10, 22, 15, 17 and 22 H_2O molecules. The information of crystal structures **1 − 5** and relevant structure refinement parameters are summarized in Table 1.

Acknowledgements

M.B. is thankful to the University Grants Commission (UGC) New Delhi, India for financial support. We thank the DST, New Delhi, India, for providing the single-crystal X-ray diffractometer facility at the Department of Chemistry, IIT Kharagpur, under its FIST program. ECS acknowledges the financial support from the Spanish Government (Grant CTQ2015-68370-P).

Keywords: coordination aggregates (CAs) • single molecule magnets (SMMs) • crystal structure • coordination environment • anisotropy

[1] (a) T. Lis, *Acta Cryst*. **1980**, *B 36*, 2042-2046. (b) D. N. Hendrickson, G. Christou, D. Gatteschi, K. Foiling, J. B. Vincent, S. Wang, A. R. Schake, H.-L. Tsai, R. Sessoli, *J. Am. Chem. Soc*. **1993**, *115*, 1804–1816.

[2] (a) C. J. Milios, A. Vinslava, W. Wernsdorfer, S. Moggach, S. Parsons, S. P. Perlepes, G. Christou, E. K. Brechin, *J. Am. Chem. Soc*. **2007**, *129*, 2754–2755. (b) A. Bencini, C. Benelli, A. Caneschi, R. L. Carlin, A. Dei, D. Gatteschi, *J. Am. Chem. Soc*. **1985**, *107*, 8128-8136. (c) C. Papatriantafyllopoulou, W. Wernsdorfer, K. A. Abboud, G. Christou, *Inorg. Chem*. **2011**, *50*, 421–423. (d) F. Habib, P.-H. Lin, J. Long, I. Korobkov, W. Wernsdorfer, M. Murugesu, *J. Am. Chem. Soc*. **2011**, *133*, 8830–8833;

[3] (a) J. D. Rinehart, J. R. Long, *J. Am. Chem. Soc*. **2009**, *131*, 12558–12559. (b) A. Ardavan, S. J. Blundell, *J. Mater. Chem*. **2009**, *19*, 1754–1760.

[4] (a) L. Bogani, W. Wernsdorfer, *Nat. Mater*. **2008**, *7*, 179-186. (b) A. R. Rocha, V. M. García-suárez, S. W. Bailey, C. J. Lambert, J. Ferrer, S. Sanvito, *Nat. Mater*. **2005**, *4*, 335–339.

[5] (a) D. Gatteschi, A. Caneschi, L. Pardi, R. Sessoli, *Science.* **1994**, *265*,1054–1058. (b) A. Ardavan, O. Rival, J. J. L. Morton, S. J. Blundell, *Phys. Rev. Lett*. **2007**, *98*, 057201–4. (c) J. Liu, Y.-C. Chen, J.-L. Liu, V. Vieru, L. Ungur, J.-H. Jia, L. F. Chibotaru, Y. Lan, W. Wernsdorfer, S. Gao, X.-M. Chen, M.-L. Tong, *J. Am. Chem. Soc*. **2016**, *138*, 5441−5450.

[6] (a) M. Murrie, S. J. Teat, H. Stœckli-Evans, H. U. Gudel, *Angew. Chem. Int. Ed*. **2003**, *42*, 4653 –4656. (b) A. K. Mondal, S. Khatua, K. Tomar, S. Konar, *Eur. J. Inorg. Chem*. **2016**, *2016*, 3545−3552. (c) C. Cadiou, M. Murrie, C. Paulsen, V. Villar, W. Wernsdorfer, R. E. P. Winpenny, *Chem. Commun*. **2001**, *24*, 2666–2667.

[7] (a) L. R. Rosado Piquer, E. C. Saňudo, *Dalton Trans*. **2015**, *44*, 8771−8780. (b) J. W. Sharples, D. Collison, *Coord. Chem. Rev*. **2014**, *260*, 1–20.

[8] (a) D. N. Woodruf, R. E. P. Winpenny, R. A. Layfield, *Chem. Rev*. **2013**, *113*, 5110−5148. (b) J. Tang, I. Hewitt, N. T. Madhu, G. Chastanet, W. Wernsdorfer, C. E. Anson, C. Benelli, R. Sessoli, A. K. Powell, *Angew.Chem., Int. Ed*., **2006**, *45*, 1729–1733. (c) S.-D. Jiang, B.-W. Wang, G. Su, Z.-M. Wang, S. Gao, *Angew. Chem*. **2010**, *122*, 7610 – 7613.

[9] (a) M. Murugesu, L. F. Chibotaru, W. Wernsdorfer, L. Ungur, G. Enright, I. Korobkov, P.-H. Lin, F. Habib, J. Long, *J. Am. Chem. Soc*. **2011**, *133*, 5319–5328. (b) M. Chen, E. C. Sañudo, E. Jimenez, S.-M. Fang, C.-S. Liu, M. Du, *Inorg. Chem*. **2014**, *53*, 6708−6714. (c) J. Tang, L. Zhao, J. Wu, M. Guo, X.-L. Li, Y,-Q. Zhang, J. Lu, *Inorg. Chem*. **2019**, *58*, 5715−5724.

[10] (a) F.-S. Guo, B. M. Day, Y.-C. Chen, M.-L. Tong, A. Mansikkamaki, R. A. Layfield, *Science* **2018**, *362*, 1400–1403. (b) C. A. P. Goodwin, F. Ortu, D. Reta, N. F. Chilton, D. P. Mills, *Nature* **2017**, *548*, 439−442. (c) F. S. Guo, B. M. Day, Y. C. Chen, M. L Tong, A. Mansikkamäki, R. A. Layfield, *Angew. Chem. Int. Ed*. **2017**, *56*, 11445–11449.

[11] (a) Y.-N. Guo, G.-F. Xu, W. Wernsdorfer, L. Ungur, Y. Guo, J. Tang, H.-J. Zhang, L. F. Chibotaru, A. K. Powell, *J. Am. Chem. Soc*. **2011**, *133*, 11948–11951. (b) R. Sessoli, A. K. Powell, *Coord. Chem. Rev*. **2009**, *253*, 2328–2341.

[12] (a) K. S. Murray, L. F. Chibotaru, B. Moubaraki, L. Ungur, N. F. Chilton, S. K. Langley, *Inorg. Chem*. **2012**, *51*, 11873−11881. (b) Z.-Q. Pan, Y.-Q. Zhang, Z.-C. Zhang, Y. Song, J. Li, H.-S. Wang, Q.-Q. Long, Z.-B. Hu, C.-L. Yin, *Dalton Trans*. **2019**, *48*, 512–522. (c) G. Rajaraman, K. S. Murray, S. K. Langley, K. R. Vignesh, *Inorg. Chem*. **2017**, *56*, 2518−2532.

[13] (a) M. Holynska, D. Premuzic, I.-R. Jeon, W. Wernsdorfer, R. Clerac, S. Dehnen, *Chem.—Eur. J*. **2011**, *17*, 9605 – 9610. (b) T. C. Stamatatos, S. J. Teat, W. Wernsdorfer, G. Christou, *Angew. Chem. Int. Ed*. **2009**, *48*, 521 –524. (c) J. Rinck, G. Novitchi, W. V. Heuvel, L. Ungur, Y. Lan, W. Wernsdorfer, C. E. Anson, L. F. Chibotaru, A. K. Powell, *Angew. Chem. Int. Ed*. **2010**, *49*, 7583 –7587.

[14] (a) M.-X. Yao, Z.-X. Zhu, X.-Y. Lu, X.-W. Deng, S. Jing, *Dalton Trans*. **2016**, *45*, 10689–10695. (b) N. Ahmed, C. Das, S. Vaidya, S. K. Langley, K. S. Murray, M. Shanmugam, *Chem. Eur. J.* **2014**, *20*, 14235 – 14239. (c) P. Kalita, J. Goura, J. M. Herrera, E. Colacio, V. Chandrasekhar, *ACS Omega*. **2018**, *3*, 5202−5211. (d) L. Rosado Piquer, E. J. Romero, Y. Lan, W. Wernsdorfer, G. Aromi, E. C. Sañudo, Inorg. *Chem. Front*. **2017**, *4*, 595–603.

[15] (a) J.-B. Peng, Q.-C. Zhang, X.-J. Kong, Y.-Z. Zheng, Y.-P. Ren, L.-S. Long, R.-B. Huang, L.-S. Zheng, Z. Zheng, *J. Am. Chem. Soc*. **2012**, *134*, 3314–3317. (b) F. Shao, J.-J. Zhuang, M.-G. Chen, N. Wang, H.-Y. Shi, J.-P. Tong, G. Luo, J. Tao, L.-S. Zheng, *Dalton Trans*. **2018**, *47*, 16850–16854. (c) E. Guarda, K. Bader, J. V. Slageren, P. Alborés, *Dalton Trans*. **2016**, *45*, 8566–8572.

[16] (a) X. Yang, Z. Li, S. Wang, S. Huang, D. Schipper, R. A. Jones, *Chem. Commun*. **2014**, *50*, 15569−15572. (b) S. K. Langley, D. P. Wielechowski, V. Vieru, N. F. Chilton, B. Moubaraki, B. F. Abrahams, L. F. Chibotaru, K. S. Murray, *Angew. Chem. Int. Ed*. **2013**, *52*, 12014 –12019. (c) F. Evangelisti, R. More, F. Hodel, S. Luber, G. R. Patzke, J. *Am. Chem. Soc*. **2015**, *137*, 11076−11084. (d) G. Maayan, G. Christou, *Inorg. Chem*. **2011**, *50*, 7015−7021.

[17] (a) P. Wang, S. Shannigrahi, N. L. Yakovlev, T. S. A. Hor, *Chem. Asian J*. **2013**, *8*, 2943–2946. (b) Z.-S. Meng, F.-S. Guo, J.-L. Liu, J.-D. Leng, M.-L. Tong, *Dalton Trans*. **2012**, *41*, 2320–2329.

[18] (a) A. Sieber, C. Boskovic, R. Bircher, O. Waldmann, S. T. Ochsenbein, G. Chaboussant, H. U. Gudel, N. Kirchner, J. V. Slageren, W. Wernsdorfer, A. Neels, H. Stoeckli-Evans, S. Janssen, F. Juranyi, H. Mutka, *Inorg. Chem*. **2005**, *44*, 4315-4325; (b) X. Qin, S. Ding, X. Xu, R. Wang, Y. Song, Y. Wang, C.-f. Du, Z.-l. Liu, *Polyhedron* **2014**, *83*, 36–43.

[19] Y. Gao, L. Zhao, X. Xu, G.-F. Xu, Y.-N. Guo, J. Tang, Z. Liu, *Inorg. Chem*. **2011**, *50*, 1304–1308.

[20] P. Wang, S. Shannigrahi, N. L. Yakovlev, T. S. A. Hor, *Dalton Trans*. **2014**, *43*, 182–187.

[21] M. Llunell, D. Casanova, J. Cirera, J. M. Bofill, P. Alemany, S. Alvarez, M. Pinsky, D. Avnir, SHAPE (2.1); Universitat de Barcelona: Barcelona, Spain, **2013**.

[22] M. Pait, A. Bauzá, A. Frontera, E. Colacio, D. Ray, *Inorg. Chem*. **2015**, *54*, 4709−4723.

[23] (a) M. A. Halcrow, J.-S. Sun, J. C. Huffman, G. Christou, *Inorg. Chem*. **1995**, *34*, 4167–4177. (b) K. Isele, F. Gigon, A. F. Williams, G. Bernardinelli, P. Franz, S. Decurtins, *Dalt. Trans*. **2007**, 332–341.

[24] (a) M. Andruh, J.-P. Costes, C. Diaz, S. Gao, *Inorg. Chem*. **2009**, *48*, 3342–3359. (b) L. Zhao, J. Wu, H. Ke, J. Tang, *Inorg. Chem.* **2014**, *53*, 3519–3525. (c) H. Ke, L. Zhao, Y. Guo, J. Tang, *Inorg. Chem*. (Washington, DC, United States) **2012**, *51*, 2699–2705.

[25] N. F. Chilton, R. P. Anderson, L. D. Turner, A. Soncini, K. S. Murray, *J. Comput. Chem.* **2013**, *34*, 1164–1175.

[26] M. Biswas, E. C. Sañudo, J. Cirera, D. Ray, *New J. Chem.* **2020**, *44*, 4812–4821.

[27] L. Rosado Piquer, S. Dey, L. Castilla-Amorós, S. J. Teat, J. Cirera, G. Rajaraman, E. C. Sañudo, *Dalton Trans*. **2019**, *48*, 12440–12450.

[28] N. F. Chilton, D. Collison, E. J. L. McInnes, R. E. P. Winpenny, A. Soncini, *Nat. Commun*. **2013**, *4*, 2551–2557.

[29] J. D. Rinehart, J. R. Long, *Chem. Sci*. **2011**, *2*, 2078–2085.

[30] S. G. Dogaheh, H. Khanmohammadi, E. C. Sañudo, *New J. Chem*. **2017**, *41*, 10101–10111.

[31] L. Yan, S. Ding, Y. Ji, Z. Liu, C. Liu, *J. Coord. Chem*. **2011**, *64*, 3531–3540.

[32] SAINT Plus, Version 7.03; Bruker AXS Inc.: Madison, WI, **2004**.

[33] Smart and XPREP; Siemens Analytical X-ray Instruments Inc., Madison, WI, **1995**.

[34] G. M. Sheldrick, SHELXT-Integrated Space-Group and Crystal-Structure Determination. Acta Crystallogr., Sect. A: Found. Adv., **2015**, *71*, 3−8.

[35] G. M. Sheldrick, Crystal Structure Refinement with SHELXL. Acta Crystallogr., Sect. C: Struct. Chem. **2015**, *71*, 3−8.

[36] O. V. Dolomanov, L. J. Bourhis, R. J. Gildea, J. A. K. Howard and H. Puschmann, *J. Appl. Crystallogr*. **2009**, *42*, 339−341.

[37] G. M. Sheldrick, SADABS: Software for empirical absorption correction, Ver. 2.05; University of Göttingen: Göttingen, Germany, **2002**.

[38] K. Bradenburg, DIAMOND, version 3.1; Crystal Impact, Bonn, Germany, **2004**.

[39] L. J. Farrugia, POV-Ray - 3.5; University of Glasgow, Glasgow, U.K., **2003**.

[40] A. L. Spek, Acta Crystallogr., Sect. C: Struct. Chem., **2015**, *71*, 9−18.